Materials Research Proceedings 28 (2023) 41-48 https://doi.org/10.21741/9781644902479-5

Development and processability of AISI S2 tool steel by laser powder bed fusion

SAGGIONETTO Enrico[1,a *], FILIPPI Elena[1,b], DEDRY Olivier [1,c], TCHUINDJANG Jérôme T.[1,d] and MERTENS Anne[1,e]

[1]Metallic Materials Science (MMS), Aerospace and Mechanical Engineering Dpt., University of Liège, Belgium

[a]enrico.saggionetto@uliege.be, [b]elena.filippi@student.uliege.be, [c]olivier.dedry@uliege.be, [d]j.tchuindjang@uliege.be, [e]anne.mertens@uliege.be

Keywords: Additive Manufacturing, Laser Powder Bed Fusion, Tool Steel, Process Map

Abstract. Nowadays, the advantages of Laser Powder Bed Fusion (LPBF) technology attract both industry and researchers. Indeed, it is possible to build up complex geometrical parts with higher mechanical properties than those obtained by conventional methods. However, LPBF involves complex phenomena due to the high heating and cooling rates that lead to out-of-equilibrium conditions. For this reason, few metal alloys are easily processable up to now. Nevertheless, research on new steels by LPBF has been growing in recent years, in particular, regarding the development of tool steels. This work thus focuses on the development of the tool steel AISI S2 by LPBF. The process map has been investigated by varying the laser power from 100 to 250 W and the scan speed from 400 to 2000 mm/s. By combining surface analysis by means of profilometer observations, density measurements by pycnometry, defects characterization and quantification and investigations on the melt pool morphology, the best process window is selected to have fully dense, defect-free parts. Furthermore, this study allows to have comprehensive insights on the effect of the parameters on the type of defects generated during the manufacturing.

Introduction

Among Additive Manufacturing (AM) technologies, Laser Powder Bed Fusion (LPBF) is a suitable technique to create near net-shape parts starting from powders. The advantage is to achieve complex parts in terms of geometry, avoiding difficult manufacturing processes. Moreover, the final mechanical properties of parts by LPBF can be higher than those obtained by conventional methods [1].

LPBF process involves complex physical phenomena, such as absorption and transmission of laser energy, rapid melting and solidification of material, microstructure evolution flow in a molten pool and material evaporation [2]. These complex phenomena may result in defects such as gas porosities, lack of fusion areas, cracks, spatters, key-hole porosities and balling [2-5]. Despite the problems and complexity faced during the process, the manufacturing of new alloys by LPBF has been growing over the recent years. Research is focusing on microstructural aspects, to gain comprehensive insights of the effect of the out-of-equilibrium conditions during melting and solidification on the final parts, both in terms of quality and mechanical properties. Significant attention has been given to the evaluation of the melt pool formed during the process [6-10], as it is crucial for understanding the processability and the type of defects generated.

Nowadays, one limitation of the LPBF process lies in the choice of raw material. Indeed, LPBF implies the use of metallic powder usually obtained by Gas Atomization (GA), a process that is difficult to control [11], especially for certain type of alloys. Therefore, few metal powders are easily available in the market (316L, Maraging Steels, Al, Ni and Ti alloys). LPBF manufacturing of other alloys has proved challenging and therefore there is a shortage of supply and demand for the less common raw material on the market.

In particular, tool steels are difficult to process by LPBF, due to their complex chemical composition and poor weldability [12]. Indeed, their high carbon content (up to 1.5 wt. %) promotes the formation of martensite, which leads to crack formation within the printed part under the effect of residual stresses due to rapid cooling. The influence of increased carbon content on LPBF processability has been investigated more deeply in recent studies [12-15]. However, other recent works already showed the possibility to manufacture low alloy steels (~ 0.5 C wt. %) [6,16-21]. The present study thus aims to provide the basis for understanding the processability of low alloy tool steel grade AISI S2. The process map for this steel is developed exploring different sets of parameters. In particular, the volumetric energy density has been used to investigate the effect of different parameters on the types of defects generated and to select the process window for fully dense and defect-free parts.

Materials and Methods

Commercial gas atomized powders AISI S2 Tool Steel (0.49 C, 1.2 Si, 0.6 Mo, 0.6 Mn, Fe bal., wt. %) were used as raw material, provided by Sandvik Osprey LTD. The powder is in a spherical shape with a mean size of 31 µm, as revealed by SEM observations (Fig. 1). The bulk density of powders (ρ_{bulk} = 7.8 g/cm^3) was measured by means of a gas pycnometer AccuPyc II Serie 1345.

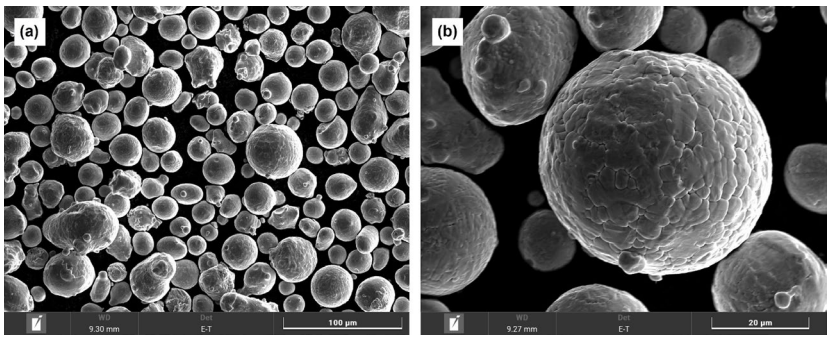

Fig. 1. SEM micrographs of (a) AISI S2 powders and (b) zoom on a particle with spherical morphology.

Starting from the powders, 20 cubes of 10x10x10 mm^3 were produced with an Aconity MIDI LPBF machine under Argon atmosphere. Different power (P) and scan velocity (v_s) were used (Table 1). P is considered as low (100 W), moderate (150 W), medium (200 W) and high (250 W). v_s is considered as low (400 - 800 mm/s), medium (800 - 1250 mm/s) and high (1250 - 2000 mm/s). A laser spot size of 80 µm with a gaussian distribution, a layer thickness (t) of 30 µm and a hatch spacing (h) of 80 µm were used for all samples. The scanning strategy implied a rotation of 90° for each layer, with no contouring. No substrate preheating was applied. Fully printed samples showed good dimensional tolerances (Fig. 2a), according to the desired initial geometrical features. Samples 1-2-3-6-11 were stopped during the manufacturing process due to evident surface defects that affect the quality of the subsequent layers (Fig. 2b-c-d). These samples were not considered for subsequent density measurements and profilometer analysis.

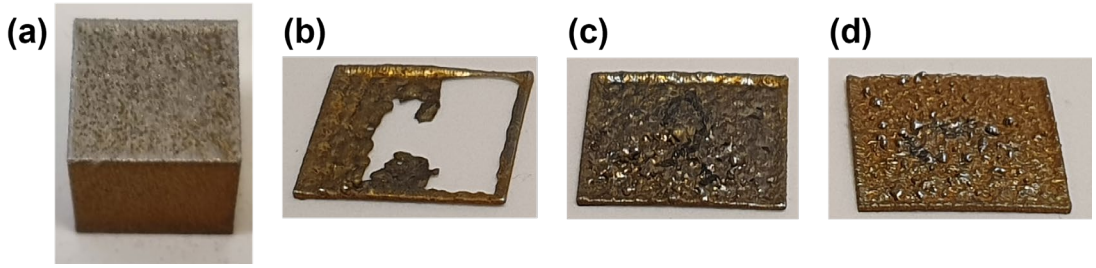

Fig. 2. Examples of (a) a fully printed and (b), (c), (d) interrupted samples.

The volumetric energy density (E_d) was used to correlate the results observed with the processing parameters (Eq. 1).

$$E_d = \frac{P}{t*h*v_s} \quad (1)$$

Table 1. Processing parameters and volumetric energy density for each sample.

Sample	P [W]	v_s [mm/s]	E_d [J/mm^3]
1	100	400	104
2	100	600	69
3	100	800	52
4	100	1000	42
5	100	1200	35
6	150	500	125
7	150	750	83
8	150	1000	63
9	150	1250	50
10	150	1500	42
11	200	500	167
12	200	750	111
13	200	1000	83
14	200	1500	56
15	200	2000	42
16	250	500	208
17	250	750	139
18	250	1000	104
19	250	1500	69
20	250	2000	52

After production, the density of each sample (ρ) was measured through a gas pycnometer and the relative density was calculated using the bulk density of powders, according to Eq. 2.

$$\%\, Density = \frac{\rho}{\rho_{bulk}} * 100 \quad (2)$$

The surface of the as-built samples was checked using an Alicona Infinite Focus G5 optical profilometer for roughness analysis. All the as-built samples were cut by Electro Discharge Machining perpendicularly to the laser scan direction of the last layer to obtain the cross section. After cutting, samples were hot mounted with an electrically conductive bakelite, then ground and polished down to 1 μm. Defects within the cross sections were analyzed through an optical microscope Olympus BX60 and quantify through Olympus Stream Analysis Software. Nital 3% was used to etch the cross sections.

Results

According to Eq. 2, all samples show a density above 96.5 %. A good correlation is observed between the density value and the fraction of internal porosity obtained by image analysis (Fig. 3a). In image analysis, all kinds of defects are considered. Small gas porosities are detected in all samples. Key-hole porosities at the bottom of melt pools are observed in samples produced with high E_d (Fig. 3b). Large spatters containing a porosity are detected in samples with low v_s (Fig.

3c). Cracks perpendicular to the building direction, initiated from the edge are detected in a few samples, without any specific correlation with processing parameters (Fig. 3d). Lack of fusion defects are visible in samples with low E_d (Fig. 3e).

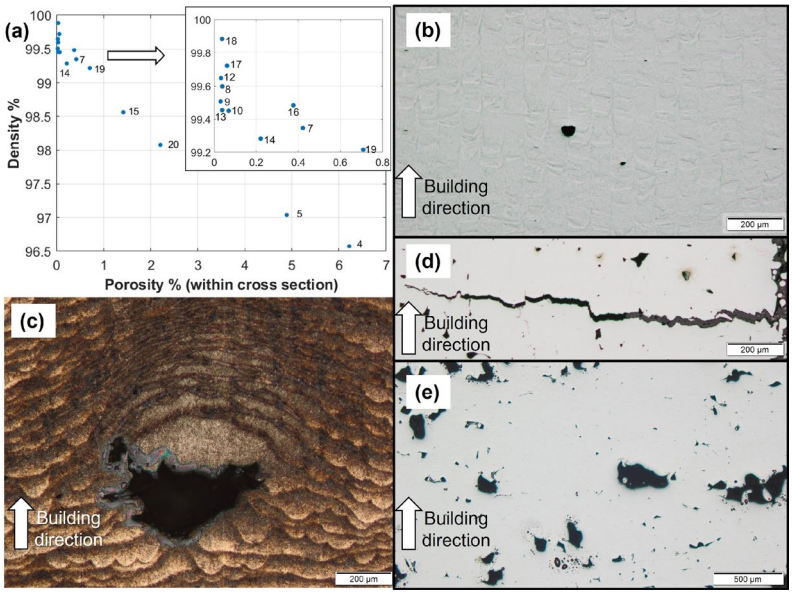

Fig. 3. (a) Correlation between density and porosity, (b) key-hole porosity, (c) entrapped porosity within large spatter, (d) crack perpendicular to the building direction initiated from sample edge and (e) lack of fusion defects.

Fig. 4 shows the most representative overviews of the sample's cross sections together with the corresponding zoom on top area. Nital etching allows to observe the features of the tracks within the sample and to distinguish the brighter top layer. The melt pool morphology is clearly visible. Increasing E_d (from left to right in Fig. 4) leads to a change in the type of defects due to a different melt pool morphology.

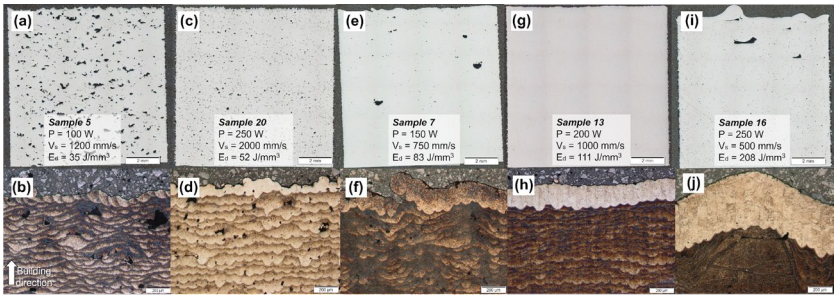

Fig. 4. (a), (c), (e), (g), (i) Cross section overviews and (b), (d), (f), (h), (j) zoom on tracks and top layer after etching with Nital.

Profilometer observations reveal different features of the surface roughness. The surface aspect depends on the quality of the scan tracks generated by the laser passage. The scan tracks generated with low E_d as result of low P (Fig. 5a) are more irregular than those obtained with high P (Fig. 5b). With intermediate value of E_d, P and v_s, the surface appears more regular, with only small spatters (Fig. 5c). On the contrary, high E_d and P and low v_s lead to an irregular surface despite the good overlapping of the scan tracks (Fig. 5e). In general, low v_s results in an irregular surface (Fig. 5d).

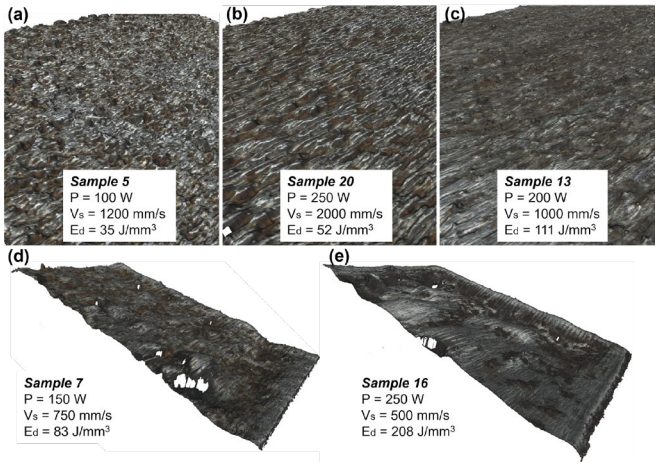

Fig. 5. Profilometer observations of the top surface after printing.

Discussion

The first approach in the LPBF of a new alloy consists in searching the best parameters to achieve fully dense and defect-free samples. Process maps are commonly used for this purpose. Although the primary aim is to obtain the best parts, investigations of defects generated using different parameters can provide good insights of both the alloy studied and the pure functioning of the LPBF process.

In this work, the effects of the two variable parameters (P and v_s) are investigated together with the variation in E_d (Eq. 1). All samples are compared in terms of density, amount and type of defects, tracks overlapping, melt pool morphology and surface quality. Particular attention is given to the quality of the top surface and the morphology of the melt pool within the top layer. Indeed, they can provide useful indications of the defects that may form in a hypothetical subsequent layer and thus understand the phenomena that have occurred in the layers below.

The use of low/moderate P (100 - 150W) and low v_s (400 - 800 mm/s) (samples 1, 2, 3, 6 and 7) does not allow for fully printed samples. The printing was stopped, excepted for sample 7. Despite the wide range of E_d (52 - 125 J/mm^3), the low P could not generate sufficient liquid phase for the powders to bond together, resulting in poor densification [3]. The metallurgical bond between layers is also compromised, leading to the possible material tear out (Fig. 2b), as also occurred in the top layer of sample 7 (Fig. 4f). Moreover, the low v_s causes an unstable melt pool generating big spatters (Fig. 2c-d) [22] that are not re-melted by the subsequent passage of the laser. If spatters are larger than the layer thickness, the spreadability of a new layer of powders is impeded, causing gaps and compromising the metallurgical layers bond [4]. Large pores (~ 400 µm) are found for instance in sample 7, that are located inside a big spatter (Fig. 3c). As the process advances, the presence of poorly printed layers leads to an irregular surface (Fig. 5d), affecting the printing of the subsequent layers.

With similar P (100 - 150 W) but higher v_s (1000 - 1250 mm/s) (sample 4 and 5), low E_d values (~ 40 J/mm^3) generate a shallow melt pool (Fig. 4b) [6]. As consequence, the metallurgical bond between two subsequent layers is compromised, causing the presence of lack of fusion areas (Fig. 4a-b) [5] that leads to low density (Fig. 3a). In this case, the poor metallurgical bond is caused by balling phenomena [3], visible in the top surface (Fig. 5a) where the tracks are clearly discontinuous. The increase in v_s is thus seen to avoid the generation of large spatters. This is easily understood since the higher v_s allows a faster cooling of the melt pool, and decreases the possibility of melted droplets being splashed out of the melt pool [22].

Low E_d values (~ 54 J/mm^3) resulting from higher P (200-250 W) and high v_s (1500-2000 mm/s) (samples 14, 15, 19, 20), leads to similar observations. Indeed, balling phenomena also occur, bringing about a low density (Fig. 3a) due to lack of fusion areas (Fig. 4c-d). However, this effect

is more restrained than observed at lower P. Indeed, the parts density is higher and the internal porosity are lower (Fig. 3a). In the present case, the higher P allows a better melting of the powders, leading to a better overlapping of the tracks as visible in the top layer (Fig. 5b). Furthermore, the melt pool height increases (Fig. 4d), allowing a better metallurgical bond with the previous layer. Therefore, the little increase of E_d (from 40 to 54 J/mm^3) results in a better processability, but the level of defects remains still high (Fig. 3a and 4c).

The combination of a moderate/medium P (150-200 W) and a medium v_s (750-1200 mm/s) (E_d = 50 - 111 J/mm^3) allows to achieve fully dense and defect-free parts (sample 08, 09, 10, 12 and 13). Indeed, this combination of parameters generate an ideal melt pool (Fig. 4h), regular and homogeneous within the cross section. The tracks have a proper overlap, which affects positively the density of the samples (Fig. 3a) and the spreadablilty of the subsequent powder layer. Indeed, no defects are found (Fig. 4g). Only small gas porosities are observed, which does not adversely affect the quality of the final part. Small spatters are visible in the top surface (Fig. 5c), but these can be easily re-melted by the subsequent laser passage. This range of parameters and especially the combination 200 W / 750-1000 mm/s (Ed ~ 97 J/mm^3) is thus considered as optimum for the realization of AISI S2 steel parts manufactured by LPBF.

Finally, high P (250 W) and low v_s (500-1000 mm/s) lead to a high E_d (104-208 J/mm^3) (sample 11, 16, 17 and 18). The deep melt pool (Fig. 4j) allows a good overlap of the tracks (Fig. 5e), resulting in high density above 99,5% (Fig. 3a). Despite this, the high E_d causes an instability of the melt pool, that is clearly irregular within the cross section (Fig. 4j). Indeed, increasing the melt pool depth also increases the possibility of gas entrapment, resulting in higher porosity. The large porosity detected (Fig. 4i) may be formed due to denudation process of powders around the melt pool due to the high E_d [2]. Key-hole defects (Fig. 3b) are also observed, formed due to the high E_d that causes metal evaporation and generate a recoil pressure towards the melt pool bottom [23]. Furthermore, the combination of low v_s and high E_d increases spattering [4], in terms of number and size of spatters. As a result, the spreadability of the subsequent layer of powders is compromised. The final part exhibits many surface irregularities, as shown by profilometer observations (Fig. 5e) and in the top layer of the cross section (Fig. 4i).

Based on the above explanations, it can be assumed that the “not processed” window (Fig. 6) results in an insufficient E_d to generate an adequate melt pool. Extensive balling and lack of fusion areas are expected due to the low P (100 - 150 W) and the high v_s (1500 - 2000 mm/s).

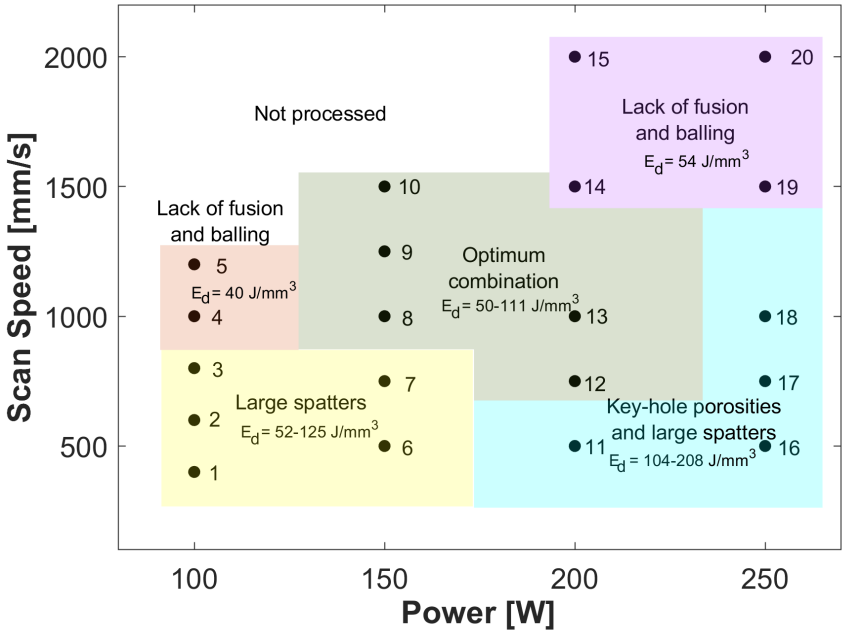

Fig. 6. Process map for AISI S2 tool steel by Laser Powder Bed Fusion.

Summary

The processability of the tool steel AISI S2 has been investigated and a process map has been built considering surface morphology, density measurements, defects characterization and quantification, tracks overlapping and melt pool morphology. The main outcomes can be summarized as follows:

- Medium v_s (750 - 1000 mm/s) and P (200 W) (Ed ~ 97 J/mm^3) allow to achieve fully dense and defect-free parts;
- High v_s (1000 - 2000 mm/s) and low E_d (35 - 69 J/mm^3) cause lack of fusion and balling, regardless of the P applied;
- Low v_s (400 - 1000 mm/s) and mostly high E_d (69 - 208 J/mm^3) cause large spatters and key-hole porosities, regardless of the P applied;

This work establishes a reference for further investigations of LPBF S2 tool steels. Furthermore, it lays the ground for the development by LPBF of new steels based on the modification of the S2 tool steel or similar grades.

Acknowledgments

This work was supported by the FNRS (Fonds National de la Recherche Scientifique of Belgium, PDR number 35298295). The authors acknowledge Sylvie Salieri for the samples preparation.

References

[1] S. Gorsse, C. Hutchinson, M. Gouné, R. Banerjee, Additive manufacturing of metals: a brief review of the characteristic microstructures and properties of steels, Ti-6Al-4V and high-entropy alloys, Sci. Technol. Adv. Mater. 18 (2017) 584-610. https://doi.org/10.1080/14686996.2017.1361305

[2] B. Zhang, Y. Li, Q. Bai, Defect Formation Mechanisms in Selective Laser Melting: A Review, Chinese J. Mech. Eng. English Ed. 30 (2017) 515-527. https://doi.org/10.1007/s10033-017-0121-5

[3] S. Chowdhury, N. Yadaiah, C. Prakash, S. Ramakrishna, S. Dixit, L.R. Gupta, D. Buddhi, Laser powder bed fusion: a state-of-the-art review of the technology, materials, properties & defects, and numerical modelling, J. Mater. Res. Technol. 20 (2022) 2109 -2172. https://doi.org/10.1016/j.jmrt.2022.07.121

[4] D. Wang, S. Wu, S. Mai, Y. Yang, Y. Liu, C. Song, Mechanisms and characteristics of spatter generation in SLM processing and its effect on the properties, Mater. Des. 117 (2017) 121 -130. https://doi.org/10.1016/j.matdes.2016.12.060

[5] J. Platl, H. Leitner, C. Turk, A.G. Demir, B. Previtali, R. Schnitzer, Defects in a Laser Powder Bed Fused Tool Steel, Adv. Eng. Mater. 23 (2021) 1-11. https://doi.org/10.1002/adem.202000833.

[6] M. A. Ryder, C.J. Montgomery, M.J. Brand, J.S. Carpenter, P.E. Jones, A.G. Spangenberger, D.A. Lados, Melt Pool and Heat Treatment Optimization for the Fabrication of High-Strength and High-Toughness Additively Manufactured 4340 Steel, J. Mater. Eng. Perform. 30 (2021) 5426-5440. https://doi.org/10.1007/s11665-021-05836-8

[7] V. Gunenthiram, P. Peyre, M. Schneider, M. Dal, F. Coste, R. Fabbro, Analysis of laser -melt pool -powder bed interaction during the selective laser melting of a stainless steel, J. Laser Appl. 29 (2017) 022303. https://doi.org/10.2351/1.4983259

[8] Q. Chen, Y. Zhao, S. Strayer, Y. Zhao, K. Aoyagi, Y. Koizumi, A. Chiba, W. Xiong, A.C. To, Elucidating the effect of preheating temperature on melt pool morphology variation in Inconel 718 laser powder bed fusion via simulation and experiment, Addit. Manuf. 37 (2021) 101642. https://doi.org/10.1016/j.addma.2020.101642

[9] Y. He, M. Zhong, N. Jones, J. Beuth, B. Webler, The Columnar-to-Equiaxed Transition in Melt Pools During Laser Powder Bed Fusion of M2 Steel, Metall. Mater. Trans. A Phys. Metall. Mater. Sci. 52 (2021) 4206-4221. https://doi.org/10.1007/s11661-021-06380-9

[10] R. Cunningham, C. Zhao, N. Parab, C. Kantzos, J. Pauza, K. Fezzaa, T. Sun, A.D. Rollett, Keyhole threshold and morphology in laser melting revealed by ultrahigh-speed x-ray imaging, Science (80-.) 363 (2019) 849 -852. https://doi.org/10.1126/science.aav4687
[11] A. L. Strauch, V. Uhlewinkel, M. Steinbacher, F. Großwendt, A. Röttger, A.B. Chehreh, F. Walther, R. Fechte-Heinen, Comparison of the processability and influence on the microstructure of different starting powder blends for laser powder bed fusion of a Fe3.5 Si1.5 C alloy, Metals 11 (2021) 1107. https://doi.org/10.3390/met11071107
[12] J. Saewe, N. Carstensen, P. Kürnsteiner, E.A. Jägle, J.H. Schleifenbaum, Influence of increased carbon content on the processability of high-speed steel HS6-5-3-8 by laser powder bed fusion, Addit. Manuf. 46 (2021) 102125. https://doi.org/10.1016/j.addma.2021.102125
[13] W. Hearn, E. Hryha, Effect of Carbon Content on the Processability of Fe-C Alloys Produced by Laser Based Powder Bed Fusion, Front. Mater. 8 (2022) 1-10. https://doi.org/10.3389/fmats.2021.800021
[14] M.A. Taha, A.F. Yousef, K.A. Gany, H.A. Sabour, On selective laser melting of ultra high carbon steel: Effect of scan speed and post heat treatment, Materwiss. Werksttech. 43 (2012) 913-923. https://doi.org/10.1002/mawe.201200030
[15] J. Kunz, M.L. Köhler, S. Herzog, A. Kaletsch, C. Broeckmann, Influence of an Increasing Alloying Content on the Microstructure of a High-Speed Steel in the Laser-Powder Bed Fusion Process, Steel Res. Int. 92 (2021), https://doi.org/10.1002/srin.202100438
[16] X. Kang, S. Dong, H. Wang, S. Yan, X. Liu, H. Ren, Effect of thermal cycle on microstructure evolution and mechanical properties of selective laser melted low-alloy steel, Materials 12 (2019) 1-15. https://doi.org/10.3390/ma12213625
[17] J.J.S. Dilip, G.D.J. Ram, T.L. Starr, B. Stucker, Selective laser melting of HY100 steel: Process parameters, microstructure and mechanical properties, Addit. Manuf. 13 (2017) 49-60. https://doi.org/10.1016/j.addma.2016.11.003
[18] W. Hearn, K. Lindgren, J. Persson, E. Hryha, In situ tempering of martensite during laser powder bed fusion of Fe-0.45C steel, Materialia 23 (2022) 101459. https://doi.org/10.1016/j.mtla.2022.101459
[19] W. Wang, S. Kelly, A Metallurgical Evaluation of the Powder-Bed Laser Additive Manufactured 4140 Steel Material, JOM 68 (2016) 869 -875. https://doi.org/10.1007/s11837-015-1804-y
[20] J. Damon, R. Koch, D. Kaiser, G. Graf, S. Dietrich, V. Schulze, Process development and impact of intrinsic heat treatment on the mechanical performance of selective laser melted AISI 4140, Addit. Manuf. 28 (2019) 275-284. https://doi.org/10.1016/j.addma.2019.05.012
[21] E. Jelis, M.R. Hespos, N.M. Ravindra, Process Evaluation of AISI 4340 Steel Manufactured by Laser Powder Bed Fusion, J. Mater. Eng. Perform. 27 (2018) 63-71. https://doi.org/10.1007/s11665-017-2989-8
[22] H. Zheng, H. Li, L. Lang, S. Gong, Y. Ge, Effects of scan speed on vapor plume behavior and spatter generation in laser powder bed fusion additive manufacturing, J. Manuf. Process. 36 (2018) 60 -67. https://doi.org/10.1016/j.jmapro.2018.09.011
[23] Y. Huang et al., Keyhole fluctuation and pore formation mechanisms during laser powder bed fusion additive manufacturing, Nat. Commun. 13 (2022) 1 -11. https://doi.org/10.1038/s41467-022-28694-x